Quantum Electronics **43** (10) 958–967 (2013)

TERAHERTZ RADIATION

PACS numbers: 42.30.Wb; 42.40.Kw; 42.25.Kb
DOI: 10.1070/QE2013v043n10ABEH014986

Application of THz probe radiation in low-coherent tomographs based on spatially separated counterpropagating beams

I.I. Kuritsyn, V.I. Mandrosov, A.P. Shkurinov, M.M. Nazarov, O.P. Cherkasova

Abstract. **A principle of designing a high-resolution low-coherent THz tomograph, which makes it possible to investigate media with a high spatial resolution (in the range λ_0–$2\lambda_0$, where λ_0 is the average probe wavelength) is considered. The operation principle of this tomograph implies probing a medium by radiation with a coherence length of $8\lambda_0$ and recording a hologram of a focused image of a fixed layer of this medium using spatially separated counterpropagating object and reference beams. Tomograms of the medium studied are calculated using a temporal approach based on application of the time correlation function of probe radiation.**

Keywords: *THz radiation, coherence, holography, tomography.*

1. Introduction

Remote determination of parameters of objects (in particular, by interferometry methods) is most often performed using highly coherent probe radiation. However, some modern tasks call for low-coherence probe radiation. An example is tomography of continuous media [1, 2], which is based on recording holograms of different layers in a medium under study. There are two versions of low-coherent tomographs aimed at solving this problem with application of probe light. One of them is a short-focus version [3], based on focused-image holography [4] according to the Gabor scheme, where the reference beam and the object beam backscattered by a medium are unidirectional [5]. According to [3], this version does not allow one to obtain high-quality tomograms of a medium at large depths from its surface because of multiply backscattered probe radiation from this medium. The second version, proposed in [6], is a long-focal-length optical scheme based on focused-image holography according to the Leith–Upatnieks scheme [7], with crossed reference and object beams. The layer-by-layer resolution in this version is one and a half higher than in the short-focus version; this difference is due to the use of long-focal-length lenses (whose aperture receives only singly scattered radiation) and probe radiation with a minimally possible coherence length $L_{cm} = 8\lambda_0$ [8], where λ_0 is the average radiation wavelength. The main drawback of all optical versions of low-coherent tomographs is that they are inefficient for media exhibiting strong light absorption. A THz version of a low-coherent tomograph based on focused-image holography, in which the reference and object beams propagate in close-to-opposite directions, was proposed in [9]. This version can efficiently be used for media characterised by much weaker absorption of THz probe radiation, for example, media with a low concentration of water molecules in the probe radiation path [10]. This tomograph implies also the use of probe radiation with a coherence length $L_{cm} = 8\lambda_0$. In this case, the reference and object beams interfere on a diffusively scattering plate, and then a significantly enlarged interference pattern is projected onto the detector matrix. However, scattering from the aforementioned plate leads to a large energy loss; therefore, this version calls for compact high-power narrowband THz sources and highly sensitive THz detectors, which are now absent. In addition, this version does not provide a maximally possible layer-by-layer resolution.

In this paper we consider a version of a low-coherent THz tomograph based on focused-image holography according to the Denisiuk scheme [11], which provides a limiting layer-by-layer resolution. In this scheme the object and reference beams are spatially separated and oppositely directed. This scheme allows one to use compact low-power THz sources with a monochromator forming probe radiation characterised by different coherence lengths L_c, including the radiation coherence length: $L_c = L_{cm} = 8\lambda_0$ [12]. The main principles of low-coherent tomography based on counterpropagating beams are analysed in Section 2. It is shown that the layer-by-layer resolution can reach $2\lambda_0$ in this case. A schematic of a long-focal-length low-coherent THz tomograph based on spatially separated counterpropagating beams is presented in Section 3. The layer-by-layer resolution of the tomographs based on counterpropagating beams and the error in determining the parameters of media studied by these tomographs are analysed in the Appendix.

2. Basic principles of low-coherent tomography based on counterpropagating beams

Let us consider a relatively simple device implementing the basic principles of low-coherent tomography based on counterpropagating beams. First, we introduce a coordinate system x, y, z (Fig. 1). Let a source (*1*) with a built-in monochromator [12] be located on the x axis and generate linearly polarised low-coherent radiation with an electric field component $E_s(t) = E_m U(t)$, where E_m is the amplitude; $U(t) = u(t)\cos[\omega_0 t + \psi(t)]$ is a dimensionless function describing the temporal evolution

I.I. Kuritsyn, A.P. Shkurinov, M.M. Nazarov Department of Physics, M.V. Lomonosov Moscow State University, Vorob'evy Gory 1, 119991 Moscow, Russia; e-mail: minotoeus@yandex.ru;
V.I. Mandrosov Moscow Institute of Physics and Technology (State University), Institutskii per. 9, 141700 Dolgoprudnyi, Moscow region, Russia; e-mail: vmandrosov@mail.ru;
O.P. Cherkasova Institute of Laser Physics, Siberian Branch, Russian Academy of Sciences, prosp. Akad. Lavrent'eva 13/3, 630090 Novosibirsk, Russia; e-mail: o.p.cherkasova@gmail.com

Received 14 September 2012; revision received 2 April 2013
Kvantovaya Elektronika **43** (10) 958–967 (2013)
Translated by Yu.P. Sin'kov

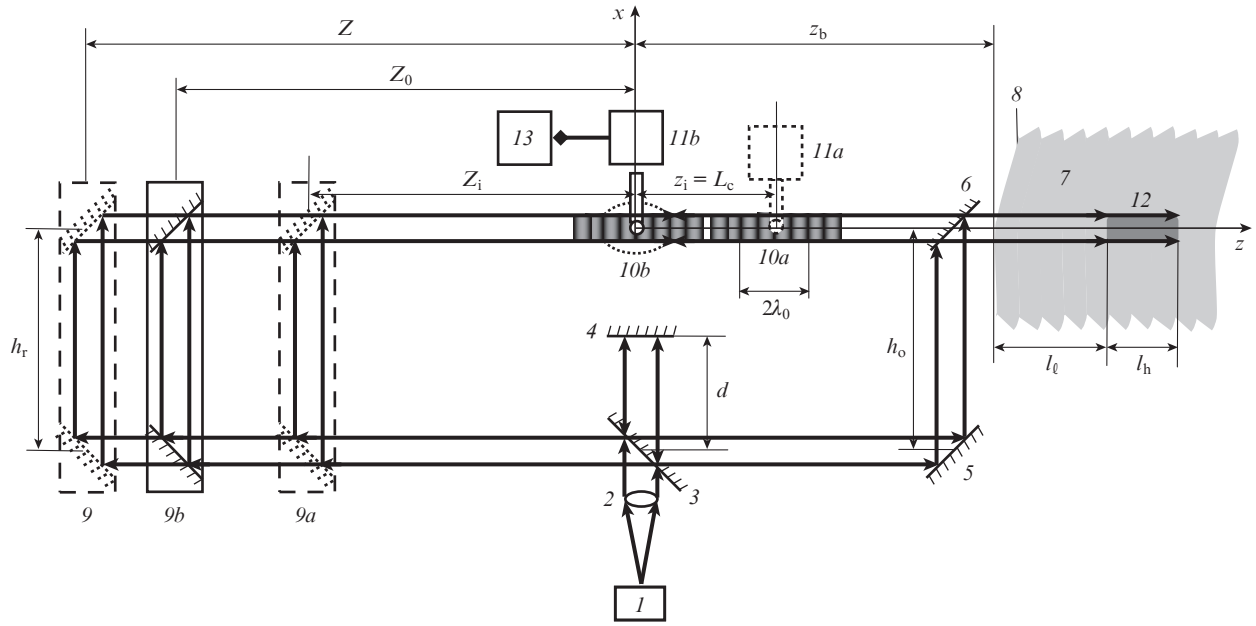

Figure 1. Block diagram of a low-coherent tomograph based on counterpropagating reference and object beams: (*1*) low-coherent radiation source; (*2*) lens; (*3*) and (*6*) semitransparent mirrors; (*4*) and (*5*) highly reflecting mirrors; (*7*) medium; (*8*) boundary of the medium; (*9a*), (*9b*) and (*9*) initial, central and current positions of the reference-beam time-delay unit; (*10a*) standing wave formed with the reference-beam delay unit in the initial position; (*10b*) standing waves formed with the reference-beam delay unit in the central and current positions; (*11a*) and (*11b*) detectors of time-averaged intensity in standing waves in the initial and fixed positions; (*12*) small inhomogeneity in the medium; and (*13*) computational device. The dotted oval shows a region of minimum size where four interference fringes of approximately equal intensity can still be formed at a probe coherence length $L_c \geqslant L_{cm} = 8\lambda_0$.

of this component; ω_0 is the high carrier frequency; $\psi(t)$ and $u(t) \leqslant 1$ are, respectively, the rapidly varying phase and slowly varying E_s modulation function; and t is the current observation time [13]. A spherical wave emitted by source (*1*) is transformed with the aid of lens (*2*) (which is also located on the x axis) into a plane wave. The latter is split into two beams by semitransparent mirror (*3*) and mirror (*4*). One of these two beams, being reflected from mirror (*5*) and semitransparent mirror (*6*), probes medium (*7*) with flat boundary (*8*) along the z axis. The probe beam reflects back from different layers of the medium to form an object beam, which interferes with an oppositely directed reference beam, formed from the second beam with a certain time delay.

To reveal the details of the formation of the interference pattern by the object and reference beams, we will consider more thoroughly the character of their propagation to the meeting point with the coordinates $x = 0$, $y = 0$ and z. The total propagation time of the probe beam and the counterpropagating object beam [reflected from boundary (*8*)] to this point is $\tau_p(z) = (2d + h_o + 2z_b - z)/c$, where d is the distance between mirrors (*3*) and (*4*), h_o is the distance between mirrors (*5*) and (*6*), z_b is the z coordinate of boundary (*8*) and c is the speed of light in air. At the same time, the reference beam is directed toward the time-delay unit (composed of two mirrors), which is depicted at three different lengths Z from the x axis (*9*), (*9a*) and (*9b*). When displacing this unit, the delay time τ_{dr} of the reference beam propagating to the same point ($x = 0$, $y = 0$, z) changes according to the law $\tau_{dr}(Z) = (2Z + h_r + z)/c$, where h_r is the distance between the mirrors forming the time-delay unit, which is equal to the distance h_o between mirrors (*5*) and (*6*). In essence, this scheme is a Mach–Zehnder interferometer, whose object and reference arms contain a reference-beam delay unit and a medium under study, respectively. As can be seen in Fig. 1, the object interferometer arm is oriented along the z axis.

Let the reference-beam delay unit be initially located at a distance $Z_i = d + z_b - z_i$ [position (*9a*) in Fig. 1], at which some fixed point with the coordinates $x = 0$, $y = 0$ and $z_i = L_c$ in the object arm of Mach–Zehnder interferometer obeys the relation $\tau_{dr}(Z_i) = \tau_p(z_i)$. Then, as was shown in [9], standing wave (*10a*) is formed around this point as a result of addition of the object- and reference-beam fields; this wave consists of interference fringes, each with a width $\lambda_0/2$. These fringes are concentrated in a fairly limited region: $z_i - L_c/4 \leqslant z \leqslant z_i + L_c/4$. At a coherence length $L_c = L_{cm} = 8\lambda_0$, standing wave (*10a*) is concentrated in a narrow range: $6\lambda_0 \leqslant z \leqslant 10\lambda_0$. Specifically this narrow region of interference of counterpropagating object and reference beams is the basic factor for implementing tomographs with a layer-by-layer resolution on the order of $2\lambda_0$ [9]. The intensity distribution in this region can be measured by displacing detector (*11a*) (with a narrow probe slid out from it) along interference fringes. When displacing the time-delay unit to the left [with respect to position (*9a*)], the interference region (and, therefore, the standing wave) should synchronously shift in the same direction. Provided that the reference-wave delay unit is displaced by the distance Z_0 from the x axis [position (*9b*) in Fig. 1], at which the relation $\tau_{dr}(Z_0) = \tau_p(z = 0)$ is satisfied, the standing wave takes position (*10b*) in the range $-L_c/4 \leqslant z \leqslant L_c/4$.

Thus, the interference pattern of the reference and object beams depends on the coordinates x, y and z and the displacement Z of the reference-wave delay unit from the x axis. Let us analyse this pattern by an example of a transparent dielectric medium with flat boundary (*8*), into which one small inhomogeneity (*12*) (also with flat boundaries) is inserted at a depth l_ℓ from boundary (*8*). In this case, the parameters z_b,

$z_\ell = z_b + l_\ell$, $z_r = z_\ell + l_h$, n_ℓ, n_h and n_r (l_h and n_h are, respectively, the thickness and refractive index of inhomogeneity (*12*), while n_ℓ and n_r are, respectively, the refractive indices of the medium on the left and on the right from the inhomogeneity) completely characterise both the position of the medium under study and its internal structure. Since n_ℓ, n_h and n_r are real numbers, the dependence of the instantaneous intensity distribution in the interference pattern on the displacement Z of the reference-wave delay unit can be written as $I(x,y,z,Z,t) = [E_r(t,x,y,z,Z) + E_o(t,x,y,z)]^2$. Here, with allowance for the fact that the boundary layers of the medium are flat,

$$E_r(t,x,y,z,Z) = E_m U[t - (2Z + z + h_r)/c] \tag{1}$$

is the instantaneous value of the electric field component in the reference beam and

$$\begin{aligned} E_o(t,x,y,z) = E_m\{&k_b U[t - (2d + h_o + 2z_b - z)/c] \\ &+ k_\ell U[t + (2d + h_o + 2z_b + 2l_\ell n_\ell z)/c] \\ &+ k_r U[t + (2d + h_o + 2z_b + 2l_\ell n_\ell + 2l_h n_h - z)/c]\} \end{aligned} \tag{2}$$

is the instantaneous value of the electric field component in the object beam (here, k_b, k_ℓ and k_r are the reflection coefficients). Furthermore, the Z value will be interpreted as the fourth coordinate of the intensity I and field E_r. It is the intensity distribution $\langle I(x,y,z,Z,t)\rangle_t$, averaged over time $T \gg \tau_c = L_c/c$ [τ_c is the coherence time of the radiation generated by source (*1*) (see Fig. 1)], that is recorded in practice. The angle brackets $\langle\ldots\rangle_t$ indicate averaging of the function $F(t)$ over time:

$$\langle F(t)\rangle_t = \frac{1}{T}\int_0^{t_0+T} F(t)\,dt,$$

where t_0 is the initial instant of averaging. When normalised to E_m^2, the distribution takes the form

$$\bar{I}_n(x,y,z,Z) = \langle I(x,y,z,Z,t)\rangle_t / E_m^2. \tag{3}$$

We will analyse the function $\bar{I}_n(x,y,z,Z)$ using the temporal approach proposed in [13], which is based on the time correlation function

$$B(\tau) = \langle U(t)U(t+\tau)\rangle_t = \cos(\omega_0\tau)\,B_u(\tau), \tag{4}$$

where $B_u(\tau) = \langle u(t)u(t+\tau)\cos[\psi(t) - \psi(t+\tau)]\rangle_t$ is the coherence function of the radiation generated by the source. The coherence function of determines its coherence time and length:

$$\tau_c = \frac{1}{T}\int_0^{t_0+T} B_u(\tau)\,d\tau, \quad L_c = c\tau_c.$$

On the assumption that $\psi(t)$ is a random process, described by the Gaussian law with a correlation time τ_ψ and standard deviation $\sigma_\psi \gg \pi$, and that $u(t) = \exp(-t^2/\tau_i^2)$, where τ_i is the width of function $u(t)$ at the level e^{-1}, the coherence function is a Gaussian: $B_u(\tau) = \exp(-\tau^2/\tau_c^2)$, where $\tau_c \approx 2\tau_i$ at $\tau_i \gg \tau_\psi/\sigma_\psi$ and $\tau_c \approx \tau_\psi/\sigma_\psi$ at $\tau_i \ll \tau_\psi/\sigma_\psi$ [8]. When $\tau_i \gg \tau_\psi/\sigma_\psi$, the radiation generated by the source is a pulse of duration τ_i, while in the case $\tau_i \ll \tau_\psi/\sigma_\psi$ the radiation is continuous. Furthermore, we assume the following conditions to be satisfied: $k_b \ll 1$, $k_\ell \ll 1$ and $k_r \ll 1$, where $k_b = (n_\ell - 1)/(n_\ell + 1)$, $k_\ell = (n_h - n_\ell)/(n_\ell + n_h)$ and $k_r = (n_h - n_r)/(n_\ell + n_r)$ are the reflection coefficients of the probe radiation from boundary (*8*) of the medium under study and from the left and right boundaries of inhomogeneity (*12*). Taking into account relations (3) and (4) and the results of [13], one can show that, at $T \gg \tau_c \gg 2\pi/\omega_0$

$$\begin{aligned} \bar{I}_n(x,y,z,Z) \approx 1 &+ k_b B_u[2(Z + z - d - z_b)/L_c] \\ &\times \cos[4\pi(Z + z - d - z_b)/\lambda_0] \\ &+ k_\ell B_u[2(Z + z - d - z_b - l_\ell n_\ell)/L_c] \\ &\times \cos[4\pi(Z + z - d - z_b - l_\ell n_\ell)/\lambda_0] \\ &+ k_r B_u[2(Z + z - d - z_b - l_\ell n_\ell - l_h n_h)/L_c] \\ &\times \cos[4\pi(Z + z - d - z_b - l_\ell n_\ell - l_h n_h)/\lambda_0]. \end{aligned} \tag{5}$$

It follows from relation (5) that the function $\bar{I}_n(x,y,z,Z)$ has maxima in both variables Z and z, with a period of $\lambda_0/2$, and the envelope of $\bar{I}_n(x,y,z,Z)$ is a surface passing through these maxima; the surface equation is determined from the relation

$$\begin{aligned} V(Z,z) = 1 &+ k_b B_u[2(Z + z - d - z_b)/L_c] \\ &+ k_\ell B_u[2(Z + z - d - z_b - l_\ell n_\ell)/L_c] \\ &+ k_r B_u[2(Z + z - d - z_b - l_\ell n_\ell - l_h n_h)/L_c], \end{aligned} \tag{6}$$

where, for a Gaussian coherence function [for which $B_u(\tau) \approx \exp(-\tau^2/\tau_c^2)$, $B_u(2Z/c) = \exp(-4Z^2/L_c^2)$].

Let the reference-beam time-delay unit be located at a distance $Z_i = d + z_b - z_i$ from the x axis [position (*9a*) in Fig.1]. Then interference fringes are formed as a result of interference of the reference beam with the object beams reflected from boundary (*8*) and from the left and right boundaries of inhomogeneity (*12*). The intensity distribution in these fringes, described by the function $E_m^2\bar{I}_{Tn}(x,y,z,Z_i)$, is measured by detector (*11a*). Measurement results can be used to construct the envelope $V(Z_i,z)$ of the function $\bar{I}_n(x,y,z,Z_i)$, which has three maxima at the points $z = z_i$, $z = z_i + l_\ell n_\ell$ and $z = z_i + l_\ell n_\ell + l_i n_i$ (where $z_i = L_c$): $V(Z_i,z_i) = 1 + k_b$, $V(Z_i,z_i + l_\ell n_\ell) = 1 + k_\ell$ and $V(Z_i,z_i + l_\ell n_\ell + l_h n_h) = 1 + k_r$. Three standing waves are formed around these points. One of these points (*10a*) is located in the interval $3L_c/4 \leqslant z \leqslant 5L_c/4$. In principle, if the values and positions of peaks of the envelope $V(Z_i,z)$ are known and the relations $k_b = (n_\ell - 1)/(n_\ell + 1)$, $k_\ell = (n_h - n_\ell)/(n_\ell + n_h)$ and $k_r = (n_h - n_r)/(n_h + n_r)$ are taken into account, one can determine all parameters of a medium studied.

Another way for determining the parameters of medium (*7*) is to fix the intensity detector in a interference fringe at the point with coordinates $x = 0$, $y = 0$ and $z = 0$ [position (*11b*) in Fig. 1] with subsequent displacement of the reference-wave time-delay unit at different distances Z from the x axis. Then detector (*11b*) will record a value E_m^2 in the initial state of time-delay unit [position (*9a*) in Fig. 1]. When this unit is displaced to the left from the initial position, three standing waves concentrated first at the points $z = z_i$, $z = z_i + l_\ell n_\ell$ and $z = z_i + l_\ell n_\ell + l_h n_h$, shift synchronously with the interference fringes forming these waves in the same direction. For example,

if the reference-wave delay unit is displaced at a distance $Z_0 = d + z_b$ from the x axis [position (*9b*) in Fig. 1], at which the relation $\tau_{dr}(Z_0) = \tau_p(z = 0)$ is satisfied, standing wave (*10a*) takes position (*10b*) to be concentrated in the interval $-L_c/4 \leqslant z \leqslant L_c/4$. According to relation (5), the dependence of the intensity recorded by detector (*11b*) on Z is determined for medium (*7*) by the function $\bar{I}_T(Z) = \bar{I}(x = 0, y = 0, z = 0, Z)$. This function, normalised to E_m^2 [$\bar{I}_{Tn}(Z) = \bar{I}_T(Z)/E_m^2$], is shown in Fig. 2a.

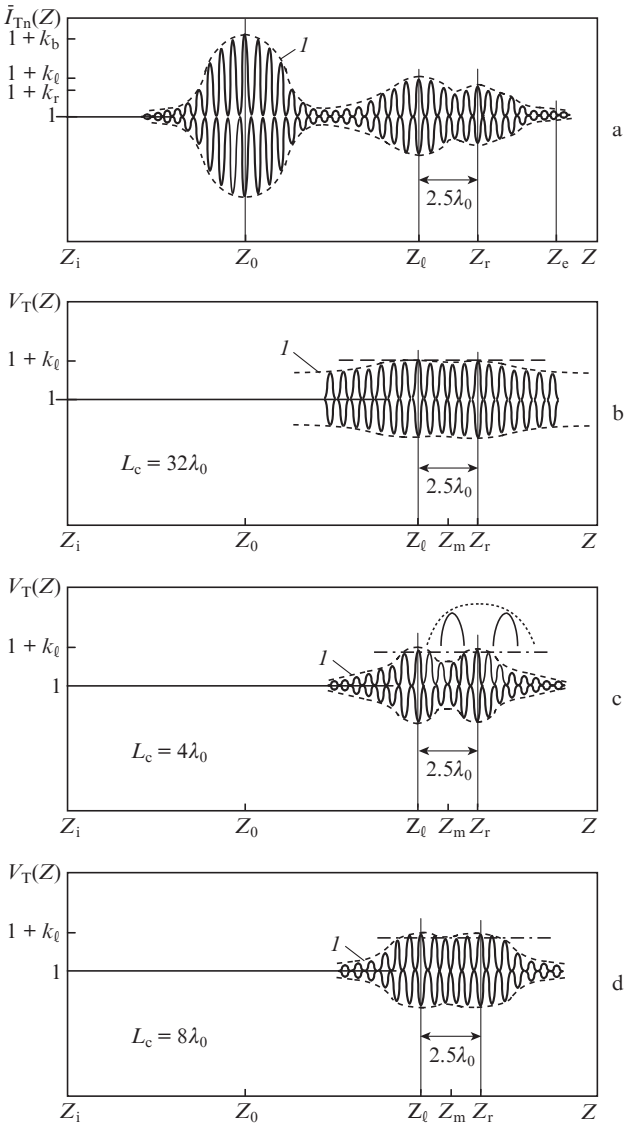

Figure 2. (a) Function $\bar{I}_{Tn}(Z)$ and (b–d) tomograms $V_T(Z)$ of medium at different probe coherence lengths L_c. (c) Case of discrepancy between the maxima of the function $\bar{I}_{Tn}(Z)$ and tomogram $V_T(Z)$.

It follows from relations (5) and (6) that the upper part of the envelope, passing through the maxima of function $\bar{I}_{Tn}(Z)$ [curve (*1*)] can be written as

$$V_T(Z) = V(Z, z = 0) = 1 + k_b B_u[2(Z - d - z_b)/L_c] + k_\ell B_u[2(Z - d - z_b - l_\ell n_\ell)/L_c] + k_r B_u[2(Z - d - z_b - l_\ell n_\ell - l_h n_h)/L_c]. \quad (7)$$

Since the function $V_T(Z)$ depends on all parameters of the medium under study, it it expedient to define this function as a tomogram of the medium. It has three maxima: $V_T(Z_0) = 1 + k_b$, $V_T(Z_\ell) = 1 + k_\ell$ and $V(Z_r) = 1 + k_r$ with the coordinates $Z = Z_0 = d + z_b$, $Z = Z_\ell = Z_0 + l_\ell n_\ell$ and $Z = Z_r = Z_0 + l_\ell n_\ell + l_h n_h$, respectively; these maxima coincide with the three largest maxima of the function $\bar{I}_{Tn}(Z)$. Note that the above relation $Z_0 = d + z_b$ was derived from the equality of the reference-beam delay time $\tau_{dr}(Z_0)$ and the propagation time $\tau_p(z = 0)$ of the object beam reflected from the boundary of the medium. Specifically due to this equality standing wave (*10a*) takes position (*10b*). Similarly, it can be shown that, when the reference-beam time-delay unit is located at distances Z_ℓ and Z_r, the standing waves concentrated first at the points $z = z_i + l_\ell n_\ell$ and $z = z_i + l_\ell n_\ell + l_h n_h$, also take position (*10b*). Based on the relations $V_T(Z_0) = 1 + k_b$, $V_T(Z_\ell) = 1 + k_\ell$ and $V(Z_r) = 1 + k_r$, $Z_0 = d + z_b$, $Z_\ell = Z_0 + l_\ell n_\ell$ and $Z_r = Z_0 + l_\ell n_\ell + l_h n_h$, $k_b = (n_\ell - 1)/(n_\ell + 1)$, $k_\ell = (n_h - n_\ell)/(n_\ell + n_h)$ and $k_r = (n_h - n_r)/(n_h + n_r)$, one can determine all parameters of medium (*7*). These are the coordinates of the medium boundary, z_b; the left and right boundaries ($z_\ell = z_b + l_\ell$ and $z_r = z_b + l_\ell + l_h$) of inhomogeneity (*12*); the refractive indices n_ℓ, n_h and n_r on the left, inside and on the right of this inhomogeneity; and the inhomogeneity thickness l_h:

$$z_b = Z_0 - d, \quad z_\ell = Z_0 - d + (Z_\ell - Z_0)[2/V_T(Z_0) - 1], \quad z_r = Z_0 - d + (Z_\ell - Z_0)[2/V_T(Z_0) - 1] + \frac{Z_r - Z_\ell}{2/V_T(Z_r) - 1}, \quad (8)$$

$$l_h = (Z_r - Z_\ell)/n_i, \quad n_\ell = [2/V_T(Z_0) - 1]^{-1}, \quad n_h = n_\ell[2/V_T(Z_\ell) - 1]^{-1}, \quad n_r = [2/V_T(Z_r) - 1]^{-1}. \quad (9)$$

The tomogram $V_T(Z)$ and the parameters of the medium under study (z_b, z_ℓ, z_r, $l_h = z_r - z_\ell$, n_ℓ, n_h and n_r) are determined by computational device (*13*) using the signals arriving from detector (*11b*).

The introduction of a probe [slid out from the housing of detector (*11b*)] into a standing wave to record the intensity distribution in it (see Fig. 1) significantly distorts this distribution. To avoid distortion, one must use a probe of thickness much smaller than the wavelength λ_0. However, such thin probes have not been developed in the THz range. Therefore, we will consider below a version of a tomograph based on counterpropagating reference and object beams, separated at a certain distance: $\Delta = h_o - h_r$. Being spatially separated, these beams do not interfere, as a result of which standing waves are not formed in this scheme. Therefore, instead of detectors for recording the intensity distribution in interference fringes (*11b*) (see Fig. 1), we propose to use detectors (*10*) and (*11*) of instantaneous values of electric field components in reference and object beams, located in the beam paths. The centre of the entrance aperture of detector (*10*) is fixed at the point with coordinates $x = 0$, $y = 0$ and $z = 0$ and the centre of the entrance aperture of detector (*11*) is at the point with coordinates $x = 0$, $y = -\Delta$ and $z = 0$. Signals from these detectors arrive at computational device (*13*).

As well as in the case described above, a tomogram of a medium under study is calculated in computational device (*13*) in the second version (compare Figs 1 and 3). Then the computational device uses the calculated tomogram to determine the coordinate of the boundary of the medium, z_b; the coordinates of the left and right boundaries (z_ℓ and z_r) of

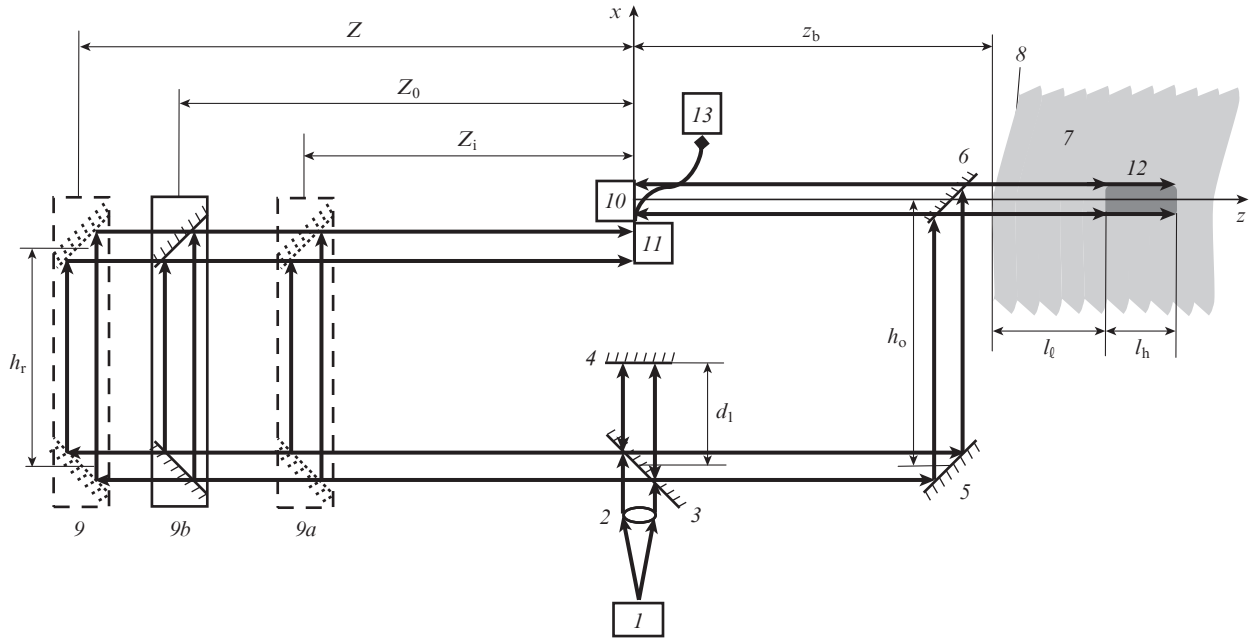

Figure 3. Block diagram of a low-coherent tomograph based on spatially separated counterpropagating reference and object beams: (*1*) low-coherent radiation source; (*2*) lens; (*3*) and (*6*) semitransparent mirrors; (*4*) and (*5*) highly reflecting mirrors; (*7*) medium; (*8*) boundary of medium; (*9a*), (*9b*) and (*9*) initial, central and current positions of the reference-beam time-delay unit; (*10*) and (*11*) detectors of instantaneous fields in the object and reference beams; (*12*) small inhomogeneity in the medium; and (*13*) computational device.

the inhomogeneity present in the medium; and the refractive indices n_ℓ, n_h and n_r on the left from the inhomogeneity, inside it and on the right from it. Note that the instantaneous field value in the reference beam is determined from the same formula (1) in both versions. In addition, on the assumption that the relation $d_1 = d - \Delta$ for the distance between mirrors (*3*) and (*4*) is satisfied in the second version, the instantaneous field in the object beam is also determined from the same formula (2) for both versions. Therefore, the function $\tilde{I}_{Tn}(x, y, z = 0, Z)$ and the tomogram of the medium in the second version are also found from formulas (6) and (7); hence, the parameters of the medium, z_b, z_ℓ, z_r, n_ℓ, n_h and n_r, are calculated from formulas (8) and (9) in the case of a tomograph based on counterpropagating, spatially separated reference and object beams (Fig. 3).

The procedure for constructing a tomogram of a medium, an analysis of the error in determining its parameters and an analysis of the layer-by-layer resolution of tomographs based on counterpropagating beams are described in Appendix. Here, we present a qualitative estimation of the error in determining the parameters of the medium for a specific case where the thickness of the inhomogeneity present in the medium obeys the inequality $l_h \leqslant 2.5\lambda_0$. As can be seen in Fig. 2b, variations in the maxima of the function $\tilde{I}_{Tn}(x, y, z = 0, Z)$ are insignificant at the coherence length $L_c = 32\lambda_0$ of the radiation generated by source (*1*). This circumstance makes it possible to determine (with a very high accuracy) the reflection coefficients k_b, k_ℓ and k_r and, as a consequence, the refractive indices n_ℓ, n_h and n_r, which are unambiguously related to the aforementioned coefficients. However, the maxima of envelope (*1*) are very wide at $L_c = 32\lambda_0$ (Fig. 2). For this reason, the deflection in the middle between the points Z_ℓ and Z_r [which allows one to distinguish the left boundary of inhomogeneity (*12*) from the right boundary] is very small. This fact indicates that the tomograph has a low resolution. The error in determining the coordinates of the left and right boundaries of the inhomogeneity (z_ℓ and z_r) and the boundary of the medium (z_b) is very large for the same reason. When the parameter L_c is small (for example, $L_c = 4\lambda_0$), variations in the maxima of function $\tilde{I}_{Tn}(x, y, z = 0, Z)$ are very large (see Fig. 2c). As a result, the error in determining the refractive indices n_ℓ, n_h and n_r is very large, although the deep deflection of the envelope between the points Z_ℓ and Z_r significantly increases the possibility of discriminating the inhomogeneity boundaries or, in other words, the resolution of the tomograph. Finally, as the Appendix shows, there is an optimal coherence length of generated radiation: $L_c = L_{cm} = 8\lambda_0$ (see Fig. 2d). In this case, variations in the maxima of function $\tilde{I}_{Tn}(Z)$ are sufficiently small, whereas the deflection of envelope (*1*) between the points Z_ℓ and Z_r is fairly large. Due to this, the high resolution of the tomograph is combined with the high accuracy in determining the inhomogeneity boundaries and the refractive indices n_ℓ, n_h and n_r. It is also shown in the Appendix that the tomograph resolution depends on the refractive index of inhomogeneity, n_h. At $L_c = L_{cm} = 8\lambda_0$, the resolution $R_T = 2.5\lambda_0/n_h$. For example, if $n_h = 1.25$, $R_T = 2\lambda_0$. This means that, at $n_h = 1.25$, a tomograph based on counterpropagating beams can determine the coordinates z_b, z_ℓ and z_r with an error $2\lambda_0$ and distinguish boundaries of an inhomogeneity of thickness $l_h = 2\lambda_0$.

3. Long-focal-length low-coherent THz tomograph based on spatially separated counterpropagating reference and object beams

The scheme presented in Fig. 3 can be used for tomography of layered media with flat irregularities at boundaries between internal layers, boundaries of the medium and inhomogeneity boundaries. In the case of steep irregularities on these surfaces (which are most often met in practice), only a very small part of the beam energy backscattered by inhomogeneity is captured by the counterpropagating reference beam. Let us consider

another version of a tomograph based on counterpropagating beams, which can efficiently be used for strongly inhomogeneous media, including layered media with steep irregularities at boundaries between layers. This is a long-focal-length low-coherent THz tomograph based on spatially separated counterpropagating reference and object beams. It is implemented as follows (Fig. 4). A source of low-coherent THz radiation (*1*) with a coherence length $8\lambda_0$ irradiates parabolic mirror (*2*) (which forms a reference beam) and the aperture of long-focal-length lens (*3*). Lens (*3*) focuses the probe radiation onto segment (*4*) of medium (*5*), which is assumed to be layered to simplify further presentation. Then long-focal-length lens (*6*) forms a convergent object beam, which provides (at the double focal distance from the lens aperture) real image (*7*) of the upper surface of layer (*8a*), located at the centre of segment (*4*). Segment (*4*) is assumed to be a parallelepiped with a height equal to the longitudinal size $l_b \approx 4\lambda_0(f/D)^2$ of the waist region of beam (*9*) and a square base with a side $l_s \approx 2\lambda_0(f/D)$, where f and D are, respectively, the focal distance and diameter of lens (*6*). Then the contour of real image (*7*) is a square with a side l_s [which is also denoted as (*7*)]. Let us introduce a coordinate system (x, y, z) with x and y axes directed along the sides of square (*7*), z axis oriented along the optical axis of lens (*6*), and origin of coordinates located at the centre of this square (at the point $x = y = z = 0$). Then the instantaneous field in the object-beam cross section, located in square (*7*), can be written as a function $E_o(t, x, y, z = 0)$ in the (x, y, z) coordinate system. The same square contains the entrance aperture of detector (*10*), which records the function $E_o(t, x, y, z = 0)$.

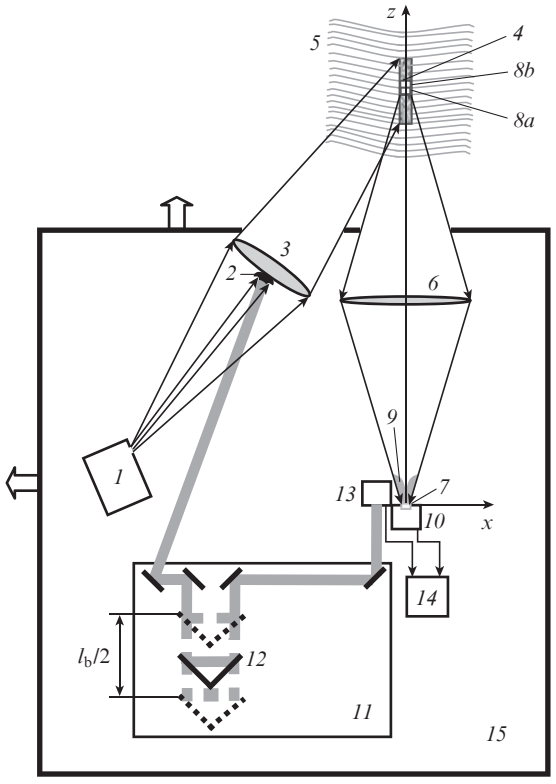

Figure 4. Block diagram of a THz long-focal-length low-coherent tomograph based on spatially separated counterpropagating reference and object beams:
(*1*) low-coherent radiation source; (*2*) parabolic mirror; (*3*) long-focal-length lens for probing segment (*4*) of medium (*5*); (*6*) long-focal-length lens forming a real image of this segment; (*7*) central cross section of the real image of segment; (*8a*) and (*8b*) segment layers located in the region that is optically conjugate with cross section (*7*); (*9*) region of the beam waist; (*10*) detector recording the instantaneous value of electric field component in the image of segment (*4*); (*11*) reference-beam time-delay unit containing four mirrors and corner reflector (*12*); (*13*) detector recording the instantaneous value of electric field component in the reference beam; (*14*) computational device forming a tomogram of the segment and determining the segment parameters from this tomogram; and (*15*) tomograph housing. Hollow arrows indicate the directions of longitudinal and transverse displacements of the tomograph housing.

The reference beam is directed [by parabolic mirror (*2*)] to unit (*11*), which contains four mirrors and mobile corner reflector (*12*); the latter changes the time delay of the reference wave by moving in the range $-l_b/4 \leqslant Z \leqslant l_b/4$, where Z is the corner reflector coordinate. The central position of the corner reflector (at $Z = 0$) is indicated by number *12* in Fig. 4. The extreme coordinates of the corner reflector, $Z = l_b/4$, are shown by dotted lines. The entrance aperture of detector (*13*) [which records the instantaneous field $E_o(t, x, y, z = 0, Z)$ in the reference beam, dependent on the current coordinate Z of the corner reflector] is in the path of the reference beam, emerging from unit (*11*) in the opposite (with respect to the object beam) direction, being centred at the point with coordinates $x = -\Delta$, $y = 0$ and $z = 0$. In this scheme, the reference-beam delay time $\tau_{dr}(Z)$ is determined by the reference-beam propagation time from mirror (*2*) to the corner reflector and then from the reflector to the entrance aperture of detector (*13*), whereas the object-beam delay time τ_p is determined by the time of propagation of the radiation probing segment (*4*) from the aperture of lens (*3*) to different layers of the medium under study located in this segment and the radiation backscattered by these layers to the entrance aperture of detector (*10*). The central position of the corner reflector ($Z = 0$) is chosen proceeding from the equality of the reference- and object-beam delay times, τ_{dr} and τ_p, when the object beam propagates from the front surface of layer (*8a*). The instantaneous field values $E_o(t, x, y, z = 0)$ and $E_r(t, x, y, z = 0, Z)$ in the object and reference beams, recorded by detectors (*10*) and (*13*), are introduced into computational device (*14*). This device calculates the total field intensity in the reference and object beams, averaged over time $T \gg \tau_c$ and normalised to E_m^2; for the transparent dielectric medium under study, this intensity is given by the relation

$$\bar{I}_{Tn}(x, y, z = 0, Z) = \langle I_n(t, x, y, Z)\rangle_t, \tag{10}$$

where $I_n(t, x, y, Z) = [E_r(t, x, y, z = 0, Z) + E_o(t, x, y, z = 0)]^2/E_m^2$. Then device (*14*) calculates the function $\tilde{I}_{Tn}^2(x, y, z = 0, Z)$, averaged over the area $S_a = \pi l_s^2$ of the entrance apertures of detectors (*10*) and (*13*):

$$\tilde{I}_{Tn}(Z) = \frac{1}{S_a}\iint \bar{I}_{Tn}(x, y, z=0, Z)\,dx\,dy. \tag{11}$$

The structure of the function $\tilde{I}_{Tn}(Z)$, as will be shown below, is similar to that of the function $\bar{I}_{Tn}(Z)$; the latter is plotted in Fig. 2a. In particular, its maxima are also determined by the object beams, which propagate from different layers of the medium. Therefore, to perform detailed analysis of the function $\tilde{I}_{Tn}(Z)$, it is expedient to divide its domain of definition, $-l_b/4 \leqslant Z \leqslant l_b/4$, into intervals h_s no wider than $6\lambda_0$. In particular, in the range from $-\lambda_0$ to $5\lambda_0$, the function $\tilde{I}_{Tn}(Z)$ corresponds to the region of layered medium (*5*), composed of two layers, (*8a*) and (*8b*) (see Fig. 4), with thicknesses

not larger than $2\lambda_0$, and their nearest vicinity. The analysis will be performed on the assumption that medium (*5*) consists of layers with fairly high irregularities on their surfaces. This means that the standard deviations of the distributions of irregularity heights $\xi_f(x,y)$, $\xi_b(x,y)$ and $\xi_m(x,y)$ on the front surface of layer (*8a*), on the rear surface of neighbouring upper layer (*8b*) and at the interface between these layers satisfy the conditions $\sigma_b \gg \lambda_0$, $\sigma_f \gg \lambda_0$ and $\sigma_m \gg \lambda_0$. We assume also that the irregularities on the layer surfaces are sufficiently steep. This means that the following conditions are satisfied: $\gamma_f = \sigma_f/\ell_f \gg D/2f$, $\gamma_b = \sigma_b/\ell_b \gg D/2f$ and $\gamma_m = \sigma_m/\ell_m \gg D/2f$, where ℓ_f, ℓ_b, ℓ_m, γ_f, γ_b and γ_m are, respectively, the correlation lengths and mean slopes of the irregularities on the upper surface of the lower fragment, on the lower surface of the upper fragment and at the interface between them. Then, to describe the parameters of layers (*8a*) and (*8b*) and their nearest vicinity, it is sufficient to use only nine parameters: the refractive index n_f of the layer adjacent to the upper surface of lower layer (*8a*); the thickness l_d and refractive index n_d of this layer; the thickness l_u and refractive index n_u of upper layer (*8b*); the refractive index n_b of the layer adjacent to the lower surface of upper layer; and the mean slopes of irregularities, γ_f, γ_b and γ_m, on the upper surface of lower layer (*8a*), lower surface of upper layer (*8b*) and the interface between them. Since layers (*8a*) and (*8b*) occupy a rather limited volume in the medium under study, the mean slopes of irregularities on their surfaces are very likely to coincide; this means that $\gamma_f = \gamma_b = \gamma_m = \sigma_m/\ell_m$. Then, it is sufficient to use only seven parameters to describe the characteristics of layers (*8a*) and (*8b*) and the adjacent layers in the medium: n_f, n_d, n_u, n_b, l_d, l_u and γ_m.

Let us now return to relation (11). To analyse it, we will take into account that lenses (*3*) and (*6*) are long-focal-length and that their optical axes make a small angle (no more than 10°). It can be shown that, under these conditions, a wave probing layers (*8a*) and (*8b*) is almost flat in their vicinity and directed along the axis of lens (*6*) and that lens (*6*) filters off an almost plane wave in region (*7*) from the waves backscattered by these layers; this wave is also directed along the axis of lens (*6*). In this case, the instantaneous field value in cross section (*7*) can be written as

$$E_o(t,x,y,z=0) \approx \alpha E_m\{k_f U[t + 2(n_f - n_d)\xi_f(x,y)/c] + k_m U[t + 2l_d n_d/c + 2(n_d - n_u)\xi_m(x,y)/c + \varphi_o] + k_b U[t + 2(l_d n_d + l_u n_u)/c + 2(n_b - n_u)\xi_b(x,y)/c]\}, \quad (12)$$

$$E_r(t,x,y,z=0,Z) = E_m U(t - 2Z/c), \quad (13)$$

where $\alpha \ll 1$ is the attenuation coefficient of the object beam due to the scattering of the radiation probing layers (*8a*) and (*8b*) from the numerous layers in medium (*5*) and the radiation propagating from these layers toward lens (*6*); $k_f = (n_f - n_d)/(n_f + n_d)$; $k_m = (n_d - n_u)/(n_d + n_u)$; $k_b = (n_b - n_u)/(n_b + n_u)$. It is noteworthy that the structure of relations (12) and (13) is similar to that of relations (1) and (2) for the instantaneous field values in the object and reference beams that are used in the tomography schemes (see Figs 1 and 2) for layered media with smooth irregularities at the layer boundaries. Furthermore we assume that the heights of irregularities $\xi_f(x,y)$, $\xi_m(x,y)$ and $\xi_b(x,y)$ have a Gaussian distribution $W(\xi) = (1/\pi\sigma)\exp(-\sigma^2/\xi^2)$ with a Gaussian correlation function $\langle \xi(x_1,y_1)\xi(x_2,y_2)\rangle_\xi = \sigma^2 \exp\{-[(x_1 - x_2)^2 + (y_1 - y_2)^2]/\ell^2\}$, where the angle brackets $\langle ... \rangle_\xi$ indicate averaging over a random value ξ. Then, using relations (10)–(13) and taking into account that, according to [14, 15], $\tilde{I}_{Tn}(Z) \approx \langle I_{Tn}(Z)\rangle_\xi$ at $\gamma_m = \sigma_m/\ell_m \gg d/2f$, one can show the following: in the range from $-\lambda_0$ to $5\lambda_0$ and with the conditions

$$\tilde{k}_f = 1/[c_m(n_f + n_d)]^2 \ll 1, \quad \tilde{k}_m = 1/[c_m(n_d + n_u)]^2 \ll 1, \quad \tilde{k}_b = 1/[c_m(n_b + n_u)]^2 \ll 1, \quad (14)$$

($c_m = \gamma_m/\alpha^2$) satisfied, the following approximate (accurate to insignificant factors) equality holds true:

$$\tilde{I}_{Tn}(Z) \approx 1 + \tilde{k}_f B_u^2(2Z/L_c)^2\cos^2(4\pi Z/\lambda_0) + \tilde{k}_m B_u^2[2(Z - l_d n_d)/L_c]\cos^2[4\pi(Z - l_d n_d)/\lambda_0] + \tilde{k}_b B_u^2[2(Z - l_d n_d - l_u n_u)/L_c]\cos^2[4\pi(Z - l_d n_d - l_u n_u)/\lambda_0]. \quad (15)$$

The parameters $\tilde{k}_f$, $\tilde{k}_m$ and $\tilde{k}_b$ in relation (15) can be interpreted as the intensity reflection coefficients from the upper surface of lower layer (*12a*), the lower surface of upper layer (*12b*) and the interface between them. They decrease with an increase in the mean slope of irregularities γ_m on the surfaces of the layers of the medium.

The envelope of the function $\tilde{I}_{Tn}(Z)$ in the range from $-\lambda_0$ to $5\lambda_0$,

$$\tilde{V}_T(Z) = 1 + \tilde{k}_f B_u^2(2Z/L_c) + \tilde{k}_m B_u^2[2(Z - l_d n_d)/L_c] + \tilde{k}_b B_u^2[2(Z - l_d n_d - l_u n_u)/L_c] \quad (16)$$

is actually a tomogram $\tilde{V}_T(Z)$ of a portion of layered medium (*5*), composed of two layers (*8a*) and (*8b*) (see Fig. 4) and their small vicinity, because it depends on the parameters n_f, n_d, n_u, n_b, l_d, l_u and γ_m, which completely determine the structure of this portion. It follows from relation (16) that the tomogram $\tilde{V}_T(Z)$ has three maxima at the points $Z_f = 0$, $Z_m = l_d n_d$ and $Z_b = l_d n_d + l_u n_u$: $\tilde{V}_T(0) = 1 + 1/[c_m(n_f + n_d)]^2$, $\tilde{V}_T(Z_m) = 1 + 1/[c_m\gamma(n_d + n_u)]^2$ and $\tilde{V}_T(Z_b) = 1 + 1/[c_m(n_b + n_u)]^2$ and that the following relations hold true if conditions (14) are satisfied:

$$\tilde{V}_T(Z_m/2) = 1 + [B_u^2(Z_m/2L_c)/c_m^2] \times [1/(n_b + n_d)^2 + 1/(n_d + n_u)^2],$$

$$\tilde{V}_T[(Z_m + Z_b)/2] = 1 + \{B_u^2[(Z_b - Z_m)/2L_c]/c_m^2\} \times [1/(n_d + n_u)^2 + 1/(n_b + n_u)^2].$$

Based on these relations, one can construct a system of seven equations,

$$\tilde{V}_T(0) = 1 + 1/[c_m(n_f + n_d)]^2,$$

$$\tilde{V}_T(Z_m) = 1 + 1/[c_m(n_d + n_u)]^2,$$

$$\tilde{V}_T(Z_b) = 1 + 1/[c_m(n_b + n_u)]^2,$$

$$Z_m = l_d n_d, \quad Z_b = l_d n_d + l_u n_u,$$

$$\tilde{V}_{\mathrm{T}}(Z_{\mathrm{m}}/2) = 1 + [B_u^2(Z_{\mathrm{m}}/2L_{\mathrm{c}})/c_{\mathrm{m}}^2] \times [1/(n_{\mathrm{b}} + n_{\mathrm{d}})^2 + 1/(n_{\mathrm{d}} + n_{\mathrm{u}})^2], \quad (17)$$

$$\tilde{V}_{\mathrm{T}}[(Z_{\mathrm{m}} + Z_{\mathrm{b}})/2] = 1 + \{B_u^2[(Z_{\mathrm{b}} - Z_{\mathrm{m}})/2L_{\mathrm{c}}]/c_{\mathrm{m}}^2\} \times [1/(n_{\mathrm{d}} + n_{\mathrm{u}})^2 + 1/(n_{\mathrm{b}} + n_{\mathrm{u}})^2]$$

with respect to seven unknowns, which are determined in device (*14*) (see Fig. 4). These are the refractive indices n_{f}, n_{d}, n_{u} and n_{b} of the portion of the analysed medium, containing layers (*8a*) and (*8b*), and the adjacent region; the mean slope γ_{m} of irregularities on the surfaces of these layers; and the thicknesses of these layers (l_{d} and l_{u}). The parameters of the neighboring portions of the medium, which correspond to the ranges $-7\lambda_0 \leqslant Z \leqslant -\lambda_0$ and $5\lambda_0 \leqslant Z \leqslant 11\lambda_0$, are determined similarly. The number of these portions in segment (*4*) and the corresponding intervals of length $h_{\mathrm{s}} = 6\lambda_0$ is determined by the relation $N_{\mathrm{d}} = l_{\mathrm{b}}/h_{\mathrm{s}} = (f/D)^2/3$. At an aperture ratio $D/f = 1/6$ for lens (*6*), $N_{\mathrm{d}} = 12$. A tomogram is calculated for each of the twelve portions of segment (*4*) in computational device (*14*), and this tomogram is used to determine the parameters n_{f}, n_{d}, n_{u}, n_{b}, l_{d}, l_{u} and γ_{m} for this portion.

Above we described in detail the procedure for determining the tomogram of one segment (*4*) of medium (*5*). The following operations are performed to obtain tomograms of other segments of this medium. First, housing (*15*), which encloses a THz long-focal-length low-coherent tomograph based on counterpropagating beams, is placed in the initial position. In this position, lens (*6*) is focused to the boundary of the initial interfacial segment with a longitudinal size l_{b} so as to form a real image of this boundary at a double focal distance from the aperture. Then the tomogram of this segment is obtained. After this procedure, the housing is shifted to the transverse direction by a value $l_{\mathrm{s}} = 2\lambda_0(f/D)$ and the tomogram of the neighbouring interfacial segment of the medium is determined. The tomograms of all segments with a longitudinal size l_{b}, located at the same depth as the initial interfacial segment, are obtained similarly. Then housing (*15*) is shifted in the longitudinal direction by $l_{\mathrm{b}} = 4\lambda_0(f/D)^2$, and tomograms of all segments with a longitudinal size l_{b}, located at a depth l_{b} from the boundary of medium (*5*), are determined. The tomograms of all segments located at a depth $2l_{\mathrm{b}}$ from the boundary of the medium are obtained in the same way, etc. It should be noted that the tomographs implemented according to the schemes depicted in Figs 3 and 4 have the same resolution and error in determining the parameters of medium. This means that a long-focal-length low-coherent THz tomograph based on spatially separated counterpropagating reference and object beams can distinguish boundaries of a layer with a thickness as small as $2\lambda_0$ from a tomogram of layered medium and determine the coordinates of boundaries of different layers with an error of $2\lambda_0$. In the THz wavelength range this means that boundaries of layers with thicknesses of 60–600 μm can be distinguished and the position of these boundaries can be determined with an error of 60–600 μm. The refractive indices of each layer can be found with a relative error of 0.06.

4. Conclusions

Tomographs based on counterpropagating beams (a kind of Mach–Zehnder interferometer, in which the object beam backscattered from a medium studied interferes with the reference beam) implement a layer-by-layer resolution equal to $2\lambda_0$ (λ_0 is the average radiation wavelength) when probing a medium by radiation with a coherence length of $8\lambda_0$. The error in determining the positions of the layer boundaries may also reach $2\lambda_0$. Based on this fact, we proposed a design of a long-focal-length THz low-coherent tomograph, which can yield information about the sizes, mean slopes of surface irregularities and the refractive indices of inhomogeneities in a medium from a tomogram of this medium; the tomogram is formed by recording field amplitudes in spatially separated object and reference beams. For layered media, the layer-by-layer resolution of this tomograph is in the range of 60–600 μm; note that the error in determining the layer boundaries also lies in this range. A low-coherent THz tomograph of this design can efficiently be used for tomography of biological media, such as nail plates, cutaneous covering, and dental tissue.

Appendix. Analysis of layer-by-layer resolution and accuracy characteristics of a tomograph based on counterpropagating reference and object beams

Let us determine the layer-by-layer resolution and accuracy characteristics of a tomograph based on spatially separated counterpropagating beams by an example of a tomograph the scheme of which is presented in Fig. 3. We will start with the construction of a tomogram of a medium under study. This procedure is based on the fact that the envelope $V_{\mathrm{T}}(Z)$ of the function $\tilde{I}_{\mathrm{Tn}}(Z)$ or, in other words, the tomogram of the medium passes through the maxima $V_{\mathrm{T}}(Z_k)$ of this function (Z_k are the coordinates of the aforementioned maxima). The coordinates Z_j of the largest maxima, $\tilde{I}_{\mathrm{Tn}}(Z_j)$, coincide with the coordinates of the maxima $V_{\mathrm{T}}(Z_j)$ of the tomogram $V_{\mathrm{T}}(Z)$. This means that the equality $V_{\mathrm{T}}(Z_j) = \tilde{I}_{\mathrm{Tn}}(Z_j)$ is valid. The other maxima of the function $\tilde{I}_{\mathrm{Tn}}(Z)$ are located symmetrically with respect to Z_j. In view of this fact, the first stage in calculation of the tomogram $V_{\mathrm{T}}(Z)$ is the search for the coordinates Z_k and the magnitudes of maxima of the function $\tilde{I}_{\mathrm{Tn}}(Z_k) = \tilde{I}_{\mathrm{Tn}}(x = 0, y = 0, z = 0, Z_k)$. Then the step approximation of the tomogram $V_{\mathrm{T}}(Z)$ is determined in the intervals $[Z_k, Z_{k+1}]$ from the relation $V_{\mathrm{T}}(Z) = V_{\mathrm{T}}(Z_k) = \tilde{I}_{\mathrm{Tn}}(Z_k)$.

Let us now take into account the influence of noise on the error in determining the parameters of medium by the example of additive noise. It can be shown that in this case the main contribution is from the noise present in the object beam, the total field in which is $E_{\mathrm{o}}(t, x, y, z) + E_{\mathrm{n}}U_{\mathrm{n}}(t)$, where E_{n} is the noise field amplitude. Here, $U_{\mathrm{n}}(t)$ is a random distribution with a correlation function $B_{\mathrm{n}} = \langle U_{\mathrm{n}}(t)U_{\mathrm{n}}(t + \tau)\rangle_t$, where the angle brackets $\langle ...\rangle_t$ indicate averaging over time t. The function B_{n} determines the correlation time

$$\tau_{\mathrm{n}} = \frac{1}{T}\int_{t_0}^{t_0+T} B_{\mathrm{n}}(\tau)\,\mathrm{d}\tau$$

of the additive noise, in the presence of which the tomogram $V_{\mathrm{T}}(Z)$ is estimated from the formula

$$\hat{V}_{\mathrm{T}}(Z_k) = \langle I_{\mathrm{S}}(x, y, z = 0, Z_k, t)\rangle_t / E_{\mathrm{m}}^2. \quad (A1)$$

Here, $I_{\mathrm{S}}(x, y, z = 0, Z_k, t) = I(x, y, z = 0, Z_k, t) + E_{\mathrm{n}}E_{\mathrm{o}}(t, x, y, z = 0) \times U_{\mathrm{n}}(t)$ and E_{m} is the amplitude of the electric field component generated by source (*1*) (Figs 1 and 3). In the absence of noise,

when $E_n = 0$, this estimate coincides with relation (3): $\hat{V}_T(Z_k) = V_T(Z_k)$. Under the conditions $\tau_n \ll \tau_c \ll T$, $k_b \ll 1$, $k_\ell \ll 1$ and $k_r \ll 1$ (k_b, k_ℓ and k_r are the reflection coefficients from the boundary of the medium and from the left and right boundaries of the inhomogeneity), which are generally performed in practice, the variance of the estimate $\hat{V}_T(Z_k)$ of the tomogram $V_T(Z)$ can be written as $D_v(Z_j) = \langle \hat{V}_T(Z_k)^2 \rangle_t - \langle \hat{V}_T(Z_k) \rangle_t^2 \approx E_n \tau_n / (E_m T)$.

It can be shown that the additive noise affects most significantly the accuracy in determining the refractive indices n_ℓ, n_r and n_h of different layers of medium studied. Hence, in the presence of additive noise, these parameters are calculated using the following estimates [rather than relation (9)]:

$$\hat{n}_\ell = 1/[2/\hat{V}_T(Z_0) - 1], \quad \hat{n}_h = n_\ell/[2/\hat{V}_T(Z_\ell) - 1], \quad \hat{n}_r = 1/[2/\hat{V}_T(Z_r) - 1]. \tag{A2}$$

It follows from (A2) that the relative error in estimating the refractive indices can be written as

$$\eta_n = (\langle \hat{n}_h^2 \rangle_t - \langle \hat{n}_h \rangle_t^2)^{1/2}/n_h = (\langle \hat{n}_\ell^2 \rangle_t - \langle \hat{n}_\ell \rangle_t^2)^{1/2}/n_\ell = (\langle \hat{n}_r^2 \rangle_t - \langle \hat{n}_r \rangle_t^2)^{1/2}/n_r = [E_n \tau_n/(E_m T)]^{1/2}. \tag{A3}$$

Relation (A3) indicates that, even in the case of noise amplitude comparable with the field amplitude, $E_n \approx E_m$, the sufficiently short noise correlation time τ_n may provide a fairly high accuracy in estimating the refractive indices n_ℓ, n_r and n_h.

Note that, even in the absence of noise, when the maxima of tomogram $V_T(Z)$ do not coincide with the largest maxima of function $\tilde{I}_{Tn}(Z)$ and the latter significantly varies in the vicinity of these maxima (a situation that is met in practice), a systematic error ΔV_s in determining $V_T(Z)$ arises. This error reaches the largest value when the maxima of function $\tilde{I}_{Tn}(Z)$ lie symmetrically with respect to the coordinates Z_j of the largest maxima of tomogram $V_T(Z)$. This case is clearly depicted in Fig. 2c, where $Z_j = Z_r$. Based on relations (5) and (7) and with allowance for $V_T(Z_r) \approx 1$, we obtain the relation $\Delta V_s = [V_T(Z_r) - V_T(Z_r \pm \lambda_0)] \approx 4k_r(\lambda_0/L_c)^2$. It can be shown that, when determining the refractive indices n_ℓ, n_r and n_h, the relative systematic error is $\eta_s = 4(\lambda_0/L_c)^2$. In particular, $\eta_s = \eta_{s1} = 1/8$ at $L_c = 4\lambda_0$, $\eta_s = \eta_{s2} = 1/32$ at $L_c = 8\lambda_0$, and $\eta_s = \eta_{s3} = 1/128$ at $L_c = 32\lambda_0$. Hence, the coherence length of the radiation generated by source (*1*) (Fig. 4) must be not smaller than $L_c = 8\lambda_0$ to provide a relative systematic error in determining the refractive indices smaller than 1/8.

Let us now analyse the resolution of a tomograph based on counterpropagating beams. We will use a tomogram of medium (*7*) (Figs 1 and 3), provided that $n_\ell = n_r$ and $Z_r = Z_\ell + 2.5\lambda_0$. In this case, the tomograms $V_T(Z_\ell)$ and $V_T(Z_r)$ have equal maxima [$V_T(Z_\ell) = V_T(Z_r)$] and the tomogram $V_T(Z)$ reaches a minimum [$V_T(Z_{min})$] in the middle of the interval $Z_\ell \leqslant Z \leqslant Z_r$, at a point $Z_{min} = Z_\ell + 1.25\lambda_0$. When the coherence length is sufficiently large ($L_c = 32\lambda_0$, see Fig. 2b), $V_T(Z_{min})/V_T(Z_r) = 0.97$. In this case, one can hardly determine the coordinates of inhomogeneity boundaries, z_ℓ and z_r, and the inhomogeneity size $l_h = z_\ell - z_r$ with acceptable accuracy, because these maxima are barely distinguishable at the aforementioned relation between the maxima $V_T(Z_\ell)$ and $V_T(Z_r)$ and the minimum $V_T(Z_{min})$. Let us define the tomograph resolution as the width of these maxima at a level of $0.85V_T(Z_\ell)$, indicated in Fig. 2c by a dot-dashed line. Then, this width is λ_0 at $L_c = 4\lambda_0$ (Fig. 2c) and $V_T(Z_{min})/V_T(Z_\ell) = 0.5$. This means that, at $L_c = 4\lambda_0$, the tomograph can reveal an inhomogeneity with a size l_h on the order of wavelength, but in this case the relative systematic error in determining the refractive indices n_ℓ, n_r and n_h of medium is fairly large: $\eta_s = 1/8$.

Let us consider an intermediate case, where the coherence length of generated radiation is $L_c = L_{cm} = 8\lambda_0$ (Fig. 2d). Under these conditions, when implementing a tomograph schematically shown in Fig. 1, one should generate a standing wave (marked by a dashed oval), the centre of which is formed by four interference fringes of almost identical intensity. As was shown in [8, 9], this is a region of minimum size in which these bands can be formed at a coherence length of probe radiation $L_c \geqslant L_{cm} = 8\lambda_0$. In this case, the width of the maxima $V_T(Z_\ell)$ and $V_T(Z_r)$ in the tomogram $V_T(Z)$ at a level of $0.85V_T(Z_\ell)$, which is indicated by a dot-dashed line in Fig. 2d, is $1.25\lambda_0$, a value corresponding to the tomograph resolution $R_T = 2.5\lambda_0/n_h$. This is a limiting resolution at which these maxima [and, therefore, both boundaries of inhomogeneity (*12*)] can be distinguished. This also means that the boundary coordinates z_ℓ and z_r are determined with a small error: $R_T = 2.5\lambda_0/n_h$. The coordinate z_b of boundary (*8*) of the medium under study is determined with the same error: $R_T = 2.5\lambda_0/n_h$. The relation $R_T = 2.5\lambda_0/n_h$ determines also the minimum thickness of inhomogeneity: $l_{hm} = R_T = 2.5\lambda_0/n_h$, which can be derived from the tomogram $V_T(Z)$. For example, if $n_h = 1.25$, $l_{hm} = 2\lambda_0$. Hence, at $n_h = 1.25$, the resolution R_T of a THz tomograph based on counterpropagating beams is in range of 60–600 μm. With a decrease in n_h of inhomogeneity (*12*), the layer-by-layer resolution of the tomograph is reduced. For example, if this inhomogeneity is an air cavity (for which $n_h = 1$), the resolution of the tomograph is $2.5\lambda_0$ and, therefore, the minimum size of inhomogeneity that can be resolved is $l_h = 2.5\lambda_0$. Thus, the layer-by-layer resolution of a tomograph based on counterpropagating beams depends on the refractive index of an inhomogeneity studied.

The proposed criterion for the resolution of a tomograph based on counterpropagating beams resembles the Rayleigh criterion, which is used to test the resolution of optics from an image of a two-point object, generated by this optics in the form of two Airy spots, specifically: the object points can be distinguished when the intensity ratio of the minimum located between these spots to the maximum in the spots is not smaller than 0.85 [14]. Thus, the condition $L_c = L_{cm} = 8\lambda_0$ provides a high accuracy in determining the coordinate of the boundary (z_b) of a medium under study, as well as the coordinates of the boundaries z_ℓ and z_r and thickness l_h of an inhomogeneity in this medium at a small relative systematic error ($\eta_s = 1/32$) in determining the refractive indices n_ℓ, n_r and n_h for different layers of this medium. This means that the case of $L_c = L_{cm} = 8\lambda_0$ is optimal for tomographs based on counterpropagating reference and object beams, including spatially separated beams. However, it can be shown that in this case, at a relative error in estimating the refractive indices n_ℓ, n_r and n_h, in the presence of additive noise $\eta_n \geqslant 3\eta_s \approx 0.1$, this noise affects the accuracy in determining refractive indices using tomographs based on spatially separated counterpropagating reference and object beams.

References

1. Bouma B.E., Tearney G.J. (Eds) *Handbook of Optical Coherent Tomography* (New York: Marcel Decker, 2002).
2. Tuchin V.V. (Ed.) *Handbook of Optical Biomedical Diagnostics* (Bellingham: SPIE Press, 2002).

3. Kirillin M.Yu., Meglinskii I.V., Priezzhev A.V. *Kvantovaya Elektron*., **36**, 247 (2006) [*Quantum Electron*., **36**, 247 (2006)].
4. Klimenko I.S. *Gologrаfiya sfokusirovannykh izobrazhenii i spekllinterferometriya* (Focused-Image Holography and Speckle Interferometry) (Moscow: Radio i svyaz', 1985).
5. Gabor D. *Nature*, **161**, 777 (1948).
6. Mandrosov V.I. *Nelineinyi Mir*, **8** (6), 361 (2010).
7. Leith E.N., Upatnieks J. *J. Opt. Soc. Am*., **54**, 1295 (1964).
8. Bakut P.A., Mandrosov V.I. *Kvantovaya Elektron*., **37**, 81 (2007) [*Quantum Electron*., **37**, 81 (2007)].
9. Mandrosov V.I. *Nelineinyi Mir*, **8** (8), 605 (2010).
10. Kuleshov E.R., Nazarov M.M., Shkurinov A.P., Tuchin V.V. *Kvantovaya Elektron*., **38**, 647 (2008) [*Quantum Electron*., **38**, 647 (2008)].
11. Denisyuk Yu.N. *Opt. Spektrosk.*, **15**, 522 (1963).
12. Cherkasova O.P., Kuritzin I.I., Mandrosov V.I., Nazarov M.M., Shkurinov A.P. *Proc. 2nd Intern. Conf. 'Terahertz and Microwave radiation: Generation, Detection and Applications' (TERA 2012)* (Moscow, 2012) p. 102.
13. Mandrosov V.I. *Kvantovaya Elektron*., **39**, 1059 (2009) [*Quantum Electron*., **39**, 1059 (2009)].
14. Mandrosov V. *Coherent Fields and Images in Remote Sensing* (Bellingham: SPIE press, 2004) Vol. PM130.
15. Born M., Wolf E. *Principles of Optics: Electromagnetic Theory of Propagation, Interference, and Diffraction of Light* (Oxford: Pergamon, 1964; Moscow: Nauka, 1973).